Available online at www.sciencedirect.com
SCIENCE DIRECT®
Journal of Nuclear Materials 329–333 (2004) 1057–1061
journal of nuclear materials
www.elsevier.com/locate/jnucmat

# Helium bubble evolution in F82H-mod – correlation between SANS and TEM

R. Coppola [a,*], M. Klimiankou [b], M. Magnani [c], A. Möslang [b], M. Valli [c]

[a] ENEA-Casaccia, FIS, CP 2400, 00100 Roma, Italy
[b] Forschungszentrum Karlsruhe, IMF-I, P.O. Box 3640, D-76021 Karlsruhe, Germany
[c] ENEA-'Clementel', V. Don Fiammelli 2, 40129 Bologna, Italy

**Abstract**

The growth of He-bubbles after low temperature He-implantation and subsequent high temperature tempering in F82H-mod steel has been studied by using transmission electron microscopy (TEM) and small-angle neutron scattering (SANS). The results obtained by both techniques show that after implantation the bubbles are homogeneously distributed around an average size of 11 Å, while after subsequent tempering He-bubbles one order of magnitude larger grow in size and volume fraction. Additionally, the SANS data show a consistent population of bubbles smaller than 10 Å, which is discussed with reference to the possible migration and coalescence mechanisms during high temperature tempering.


## 1. Introduction

Moving towards the development and world-wide optimisation of reduced-activation 8–9Cr2WVTa steels, some encouraging results have become available on the critical issue of low temperature irradiation hardening and embrittlement. Various data sets on neutron irradiated heats are showing that within wide temperature and displacement damage dose ranges these steels are also favourable with respect to a general improvement of the fracture toughness properties [1]. However, whether helium generated by inelastic (n,α)-processes will have a significant effect on impact properties, such as the ductile–brittle transition temperature or the lifetime and reliability of fusion structural materials, is the subject of ongoing discussions [2–4]. The demonstration of a direct relationship between helium and embrittlement based on fast or mixed spectrum fission reactors is difficult because such simulation techniques require alloying with B-10 or Ni-59 for the helium production.

Since morphology, distribution and growth mechanisms of helium bubbles can sensitively determine the microstructural reasons for embrittlement effects, their size distribution functions as well as temperature stability must be determined. Transmission electron microscopy (TEM) investigations enable direct observation of He-bubbles and deliver reliable data concerning local bubbles morphology and spatial distribution, but their resolution limit is approximately 10 Å for He-bubbles in magnetic Fe-alloys. Small-angle neutron scattering (SANS) is therefore an appropriate technique to investigate this phenomenon, as also shown by previous studies [5,6], and to complement the microstructural information obtained by TEM, which is the subject of this paper.

## 2. Experimental

The chemical composition of the investigated F82H-mod steel is: 8.0 Cr, 0.10 C, 0.16 Mn, 0.16 V, 2.0 W, 0.02 Ta (in wt%). Samples given an initial standard heat treatment have been homogeneously implanted with 400 appm He at 250 °C, using the 104 MeV α-particle beam of the cyclotron facility at FZ-Karlsruhe [7]. In order to obtain information on He-bubble growth as a function

* Corresponding author. Tel.: +39-06 30484724; fax: +39-06 30484747.
*E-mail address:* coppolar@casaccia.enea.it (R. Coppola).

0022-3115/$ - see front matter © 2004 Elsevier B.V. All rights reserved.
doi:10.1016/j.jnucmat.2004.04.134

of the temperature, after implantation the samples were submitted to 2 h tempering (at 525, 825 and 975 °C) in high vacuum, together with non-implanted reference samples. For the case of as-implanted sample, the thermal reference was provided by a sample of the same material tempered at 250 °C for a time equivalent to the irradiation time (5 days). The TEM investigations were performed on the PHILIPS T400 100 KV acceleration voltage equipped with $LaB_6$ cathode in the 'hot-cells' FZ-Karlsruhe. The TEM samples were prepared, after the SANS measurements were completed, by usual electrochemical etching and then cut under the shape of disks of 1 mm diameter, using a special sample holder for the observations. This procedure minimises the magnetic volume and facilitates the TEM adjustment, enabling the observation of He bubbles with a minimum size (apparent diameter) of approximately 10 Å.

Reference is made to [8] and to previous work [5,6] for a general presentation of SANS and of its application to the study of martensitic steels. The SANS measurements were carried out by means of the D22 instrument at the High Flux Reactor of the Institut Laue Langevin, Grenoble. A sample-to-detector distance of 8.00 m with a wavelength $\lambda$ of 6 Å was used. Combined with the previous SANS measurements carried out on these same samples [5,6] this gave a $Q$ interval (the modulus of the scattering vector being $Q = 4\pi \sin\theta/\lambda$, where $2\theta$ is the full scattering angle) ranging from 0.007 to 0.25 $Å^{-1}$, which corresponds to particle sizes ranging from 10 to 150 Å approximately. The size distributions were determined by indirect transformation of the SANS cross-section:

$$d\Sigma(Q)/d\Omega = (\Delta\rho)^2 \int_0^\infty dR N(R) V^2(R) |F(Q,R)|^2, \qquad (1)$$

where $N(R)$ is the number per unit volume of centers with a typical size between $R$ and $R + dR$ (the volume distribution function is $D(R) = N(R)R^3$), $V$ their volume and $|F(Q,R)|^2$ their form factor (assumed spherical in this case) and $(\Delta\rho)^2 = (\rho_{He} - \rho_{F82H})^2 = 4.833 \times 10^{21}$ $cm^{-4}$ is the 'contrast' or square difference in neutron scattering length density between He-bubbles, $\rho_{He} = 0.588 \times 10^{10}$ $cm^{-2}$ and the F82H-mod matrix, $\rho_{F82H} = 7.54 \times 10^{10}$ $cm^{-2}$, the latter being determined from the chemical composition of F82H-mod steel [6,8]. The contrast dependence on bubble radius [9] was taken into account [10], but as already discussed in a previous work [6] the effect of this correction on the distributions is of a few %, that is well below the experimental uncertainties. Furthermore it is evident from the small value of $\rho_{He}$ that very large changes of the He mass density would be necessary to lead to significantly different distributions. Eq. (1) was solved using the method reported in Ref. [11] and more recently discussed in Refs. [6,12], where the influence of background subtraction and the reliability of information referring to inhomogeneities corresponding to $Q$-values outside the available experimental range are more specifically addressed.

## 3. TEM results

In all the investigated samples the TEM observations show clearly the presence of He-bubbles, visible in Fig. 1; the corresponding histograms, average radii and volume fractions are presented in the next section. In the as-implanted sample the size of the bubbles range from 8 to 22 Å with an average of 14 Å, in excellent agreement with previous TEM observations [13]. The small bubbles are more easily visible on the image out of defocus [14]. In an underfocus condition the cavity image is bright relative to the background and the image has a dark rim. The reverse is true in overfocus condition when the bubble is a dark image with a faint bright rim. Fig. 2 shows two micrographs from the as-implanted sample taken at underfocus adjustment with $\Delta f = -600$ Å and overfocus adjustment with $\Delta f = +800$ Å, both displaying the same pattern of He-bubbles: the very similar pattern of bright and dark spots confirms that the He bubbles and not noise are imaged. The rim decorating the bubbles through their perimeter originates from Fresnel fringes at the boundaries between two phases and its image defines the real cavity diameter. The size of the fringes is generally 10–20 Å, which can lead to an

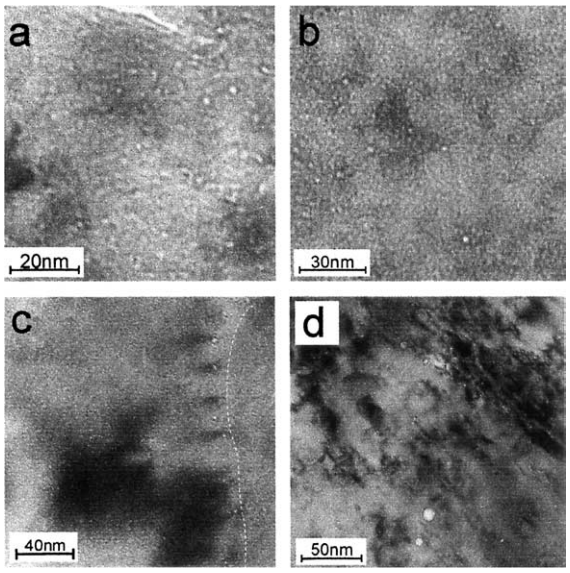


Fig. 1. TEM micrographs of the He-bubbles in F82H-mod as-implanted at 250 °C (a) and after tempering at 525, 825 and 975 °C ((b)–(d) respectively).

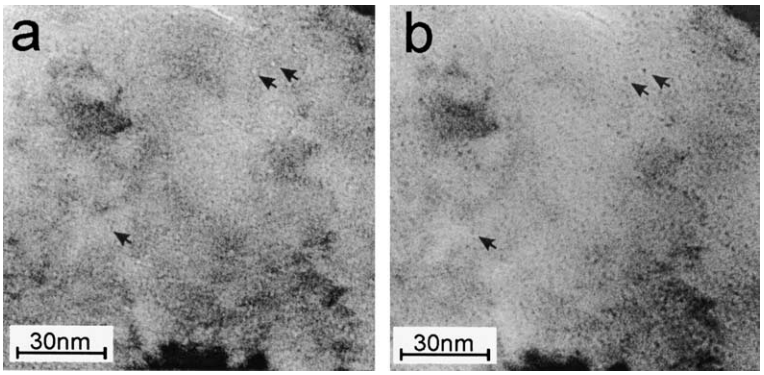


Fig. 2. TEM micrographs of the He-bubbles in the as-implanted sample taken at underfocus (a) and overfocus (b) adjustment.

error in the measurement of the bubbles size, increasing significantly for the smaller sizes.

The sample tempered at 525 °C (Fig. 1(b)) appears similar to the as-implanted one, with He-bubbles homogeneously distributed, ranging from 10 to 40 Å in size: clearly, a coarsening has not yet started and no significant difference is found with respect to the as-implanted specimen.

A remarkable increase in the size and number of the He-bubbles is observed in the sample tempered at 825 °C (Fig. 1(c)). The bubbles are not always homogeneously distributed, but often located along internal interfaces like prior austenite grain boundaries. As an example, the boundary decorated in the vicinity with He bubbles is marked with a white broken line on the right side of the micrograph. The size of the bubbles ranges from 10 to 100 Å with an average of 30 Å. For sizes lower than about 50 Å, the size distribution is very approximately a Gaussian (like in the as-implanted and in the 525 °C tempered samples).

A further growth of the He bubbles is observed after tempering at 975 °C (Fig. 1(d)). The corresponding histogram is broad and non-Gaussian, with sizes ranging from less than 30 Å up to 280 Å (peaked around 40 Å): clearly, this is not only a continuation of the growth processes observed at 825 °C, but it reflects a substantial acceleration of bubble growth kinetics. The spatial distribution of the He-bubbles is quite inhomogeneous and it is also obvious that in spite of the high tempering temperature, far beyond the upper operation temperature, still a significant fraction of the bubbles is observed in the matrix.

## 4. SANS results

The best-fit $D(R)$ distributions at 250, 825 and 975 °C are shown in Fig. 3, compared in the overlap region with the corresponding TEM histograms. The corresponding He bubbles average radii and volume fractions are reported in Table 1. At 525 °C the difference in SANS cross-section between implanted and reference sample is smaller than the experimental errors, as already found in the previous experiment [5,6]: that has been tentatively attributed to the slight differences in the thermal history of the two samples and to the occurrence of a dense, fine precipitation of the $M_2C$ phase around this temperature [15]. The fact that no significant difference is observed by TEM between the as-implanted sample and the one tempered at 525 °C after implantation further supports this interpretation. In agreement with the previous results, the best-fit distributions of Fig. 3 show that after implantation the bubbles are quite small and homogeneously distributed in size (Fig. 3(a)), while after tempering they increase in size and volume fraction with increasing temperature: these new SANS measurements, extended towards significantly smaller $Q$-values, provide more detailed and reliable information on the larger bubbles. The comparison with the TEM histograms, presented in the three insets of Fig. 3, is made reporting the $D(R)$ distributions only for sizes larger or equal to those detectable by TEM, where there is a good correlation between SANS and TEM. The SANS data show additionally a high density of bubbles with sizes below the resolution limit of TEM. It is however noted that the SANS resolution too strongly decreases below 10 Å, as is also shown by the correspondingly large error bands, mostly because of the background arising from the matrix; consequently, quantitative information on the true shape of the distributions can hardly be obtained for the smaller radii region. For this same reason, for $R < 10$ Å errors as high as 40–50% are estimated [5,6] on the He-bubble volume fraction and average radii, which are summarized in Table 1. More specifically, no quantitative conclusion can be based on the very small, mathematically averaged radii determined at 825 and 975 °C.

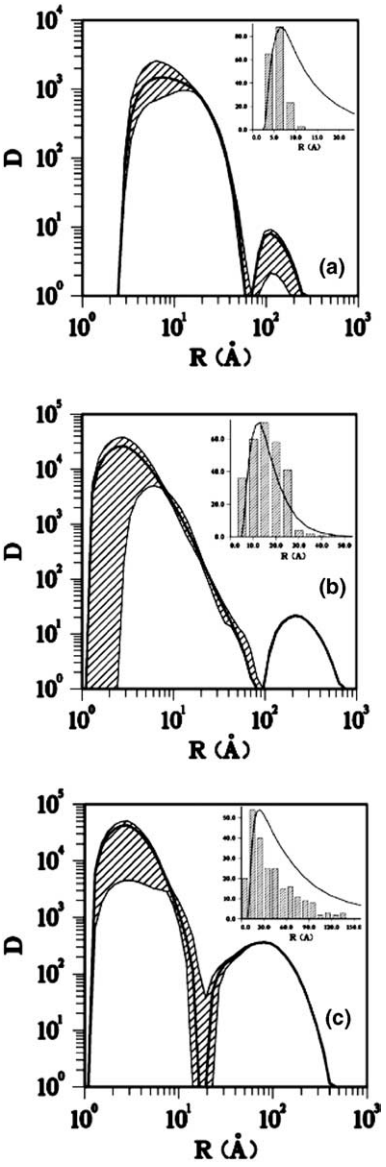


Fig. 3. Best-fit He-bubble volume distributions $D(R)$ in $Å^{-1}$ in F82H-mod steel as-implanted at 250 °C (a), 825 °C (b), 975 °C (c). The dashed area represents the 80% confidence band. For each temperature, the comparison with the corresponding TEM histogram is shown in the upper right corner: the relative intensities of SANS and TEM data (insets), in arbitrary units, are normalised by their respective maxima.

## 5. Discussion and conclusions

Assuming that after high temperature tempering all implanted helium would be concentrated in detectable equilibrium bubbles, $\Delta V$ should reflect the implanted helium concentration

Table 1
He bubble volume fraction, $\Delta V$, and average radius $R_b$ (Å) from SANS data; at 825 and 975 °C the $R_b$ values in italics are averaged on the portion of the $D(R)$ compared with the TEM histograms in the insets of Fig. 3

| Tempering temperature (°C) | $\Delta V$ | | $R_b$ (Å) |
|---|---|---|---|
| 250 | 0.0012 (0.0039) | | 11.2 (7) |
| 825 | 0.0053 (0.0036) | 3.8 | *14.1* (17) |
| 975 | 0.0085 (0.0054) | 4.1 | *47.9* (46) |

The $R_b$ and $\Delta V$ values in parentheses are those obtained from TEM.

$$C_{He} = \gamma \frac{\Delta V}{R_b} \frac{\Omega}{kT}, \tag{2}$$

where $\gamma$ is the bubble surface energy (related to He pressure $p_{He} = 2\gamma/R_b$ and assumed $\gamma = 1$ J/m$^2$), $\Omega = 0.5 \times 2.87$ Å$^3$ is the atomic volume and $k = 1.38 \times 10^{-23}$ J/K [16]. Inserting into Eq. (2) the smaller average radii values of Table 1 and neglecting the 'large' bubble population gives concentration values about one order of magnitude larger than the nominal one (400 appm): as it has previously been discussed [6], that may imply that the effect of the background is partly underestimated, enhancing correspondingly the very low-$R$ portion of the volume distributions, although with a consistent error band. On the other hand, the presence of He-bubbles smaller than 10 Å is clearly indicated by the SANS data, therefore it should also be considered that such small bubbles might not be in equilibrium and consequently Eq. (2) would not hold. The present results confirm and complete the previous findings on He-bubble growth in implanted F82H-mod steel. In the as-implanted material both SANS and TEM show a homogeneous and narrow distribution of bubbles approximately 11 Å in average radius. After high temperature tempering TEM reveals in agreement with SANS higher average bubble sizes, increasing with the temperature. At 975 °C, that is above the $\alpha \rightarrow \gamma$ transition temperature, both TEM and SANS show a very broad range of bubble sizes as large as 250 Å, with unusual distribution function, possibly attributed to Brownian type motion and coalescence during isochronal tempering. The high density of bubbles below the TEM resolution limit, shown by the SANS results, might suggest the existence of a high density of vacancy clusters produced as one of the end-products of subcascades created by higher energy PKA's. He atoms would therefore be trapped and stabilise these already existing vacancy clusters. In any case, as substantial bubble growth in short times does not appear before annealing beyond the $\alpha \rightarrow \gamma$ transition temperature, any temperature excursion beyond 780–820 °C (as should be produced by joining or

plasma disruptions) of reduced activation ferritic/martensitic steels containing He should be avoided. Not only would substantial swelling occur in the fcc phase but also long range migration of He and substantial bubble growth at the grain boundaries would occur, which in turn would lead to high temperature He embrittlement. Once few but large bubbles have grown up in the fcc phase they remain stable after subsequent cooling below the the $\alpha \rightarrow \gamma$ transition temperature.

## Acknowledgements

Dr R.P. May (ILL) is gratefully acknowledged for valuable help in running the SANS experiment and for scientific discussions.

## References

[1] A. Hishinuma, A. Kohyama, R.L. Klueh, D.S. Gelles, W. Dietz, K. Ehrlich, J. Nucl. Mater. 258–263 (1998) 193.
[2] R.L. Klueh, D.J. Alexander, J. Nucl. Mater. 218 (1995) 151.
[3] E. Materna-Morris, M. Rieth, K. Ehrlich, in: M.L. Hamilton et al. (Eds.), Proceedings of the 19th International Symposium on Effects of Radiation on Materials ASTM STP 1366, 1999, p. 597.
[4] R. Lindau, A. Möslang, D. Preininger, M. Rieth, H.D. Röhrig, J. Nucl. Mater 271&272 (1999) 450.
[5] R. Coppola, M. Magnani, R.P. May, A. Möslang, J. Appl. Cryst. 33 (2000) 469.
[6] R. Coppola, M. Magnani, R.P. May, A. Möslang, M. Valli, J. Nucl. Mater. 283–287 (2000) 183.
[7] A. Möslang, S. Cierjacks, R. Lindau, in: B. Martin, K. Ziegler (Eds.), Proceedings of 12th International Conference on Cyclotrons and their Applications Berlin 1989, World Scientific, London, 1991, p. 545.
[8] M.T. Huthchings, C.G. Windsor, in: K. Sköld, D.L. Price (Eds.), Methods of Experimental Physics, vol. 23-c, Neutron Scattering, Academic, 1987, p. 405.
[9] Qiang-Li, W. Kesternich, H. Schroeder, D. Svhwahn, H. Ullmaier, Acta Metall. Mater. 38 (1990) 2383.
[10] To be published elsewhere by the same authors.
[11] M. Magnani, P. Puliti, M. Stefanon, Nucl. Instrum. and Meth. A 271 (1988) 611.
[12] R. Coppola, R. Kampmann, M. Magnani, P. Staron, Acta Mater. 46 (15) (1998) 5447.
[13] J. Bertsch, FZK Report 5984, 1997.
[14] J. van Langduyt, R. Gevers, S. Amelinckx, Phys. Stat. Sol. 10 (319) (1965).
[15] R. Coppola, K. Ehrlich, M. Magnani, E. Materna-Morris, M. Valli, J. Nucl. Mater. 258–263 (1998) 1291.
[16] G. Bürkle, A. Möslang, unpublished Internal FZK Report 02.02.02P68A, 1997.